

Design and Simulation of Micro-Electro-Mechanical Systems (MEMS) Capacitive Pressure Sensor for Thermal Runaway Detection in the Electric Vehicle

H. M. M Hajizi¹, H. Aris^{1,2,*}, W. M. W. Norhaimi^{1,2}, N. I. M. Nor^{1,2}, Z. Sauli^{1,2}, and A. A. Aziz³

¹Faculty of Electronic Engineering & Technology, Universiti Malaysia Perlis (UniMAP),
02600 Arau, Perlis, Malaysia

²Centre of Excellence for Micro System Technology (MiCTEC), Universiti Malaysia Perlis (UniMAP),
02600 Arau, Perlis, Malaysia

³Integrated Microelectronic System and Application Research Group, School of Electrical Engineering,
College of Engineering, Universiti Teknologi MARA, 40450 Shah Alam, Selangor, Malaysia

ABSTRACT

Recent advancement of vehicle technologies has resulted in development of replacing conventional Internal combustion engine (ICE) to Electric Vehicle (EV) mostly powered by Lithium-ion batteries (LIB). These batteries contain massive amount of energy confined in a very small space. Thermal runaway occurs when the batteries and its circuits start to heat up anomaly. Thermal runaway can cause failures that can lead to battery ignition, resulting in explosions and imminent threats to life and property. This research focused on MEMS capacitance pressure sensor, using three distinct square slotted diaphragm designs: clamped-square, four-slotted-square, and eight-slotted-square diaphragms. The investigation commenced with an evaluation of diaphragm performance, and subsequently, the diaphragm was integrated into the structure of the MEMS capacitive pressure sensor and subjected to simulation. Varied pressure levels ranging from 0.1 to 0.35 MPa were applied to both the diaphragm and the pressure sensor. The outcomes revealed that the eight-slotted-square diaphragm yielded the most substantial displacement, registering at 5.507 μm . It also exhibited the highest Mises stress of 644.67 MPa, and recorded the highest mechanical sensitivity at 15.7545 ($10^{-12}/\text{Pa}$). The clamped-square design, despite its slotted area, yielded the highest capacitance value among the three designs for the pressure sensor.

Keywords: MEMS capacitive pressure sensor, thermal runaway, electric vehicle

1. INTRODUCTION

The global sales of EVs have been steadily increasing in recent years. The global EV market has been expanding steadily over the past decade, driven by factors such as government incentives, stricter emissions regulations, advancements in battery technology, and increased consumer interest in sustainable transportation. An electric vehicle, commonly known as an EV, is a type of vehicle that is powered by electricity rather than traditional internal combustion engines (ICE) that run on petroleum like gasoline or diesel. EVs utilize electric motors and rechargeable batteries to provide propulsion [1]. There are different types of EVs available on the market. Battery Electric Vehicles (BEVs) are fully electric and solely rely on batteries for power. Plug-in Hybrid Electric Vehicles (PHEVs) combine an engine with an electric motor and battery, offering the option to run on electricity or conventional fuels. Additionally, there are also Hybrid Electric Vehicles (HEVs), which use both an internal combustion engine and an electric motor, but un-rechargeable.

* Corresponding authors: hasnizah@unimap.edu.my

In terms of safety, battery fire and electrical safety is a major drawback of EV from becoming the preferred transportation system [2]. Since the introduction of EV, a worrying number of fire incidents has taken place and most of these incidents are caused by self-ignition, where the fire occurs in the battery system itself. The change in physical shape of the batteries introduces immense pressure to the battery cell that leads to the primary trigger to cell rupture within leads to smoke, fire, and ultimately explosion, posing imminent threats to the lives and properties of human being.

Despite meeting all specification and safety regulations, the practical implementation of LIB in real-world conditions and environment still presents a significant challenge in eliminating the potential occurrences of thermal runaway event. Enhancing the reliability of the battery and improvement of the efficiency of temperature sensing would be two viable solutions to mitigate the fire incident. The implementation of early-warning mechanism through continuous monitoring is essential and the most effective ways to prevent such scenario.

The primary focus of this report will be the introduction of thermal runaway detection system within the battery packs, aimed at identifying instances of battery failure. Currently, Battery Management System (BMS) is used as an electronic system to monitor and control the charging, discharging, and overall operation of rechargeable batteries. BMSs are commonly used in various applications, including EVs, renewable energy systems, portable electronics, and energy storage systems. Its primary functions are including voltage, current, and temperature monitoring of battery, the state of charge of the battery, cell balancing, charge and discharge controls, thermal management, fault diagnosis and protection and some of manufacturer even incorporate communication interfaces in the BMS. Despite the potential of pressure elevation that could potentially affect the efficiency of heat dissipation, a pressure sensor is typically not included in the BMS configuration.

In the event of pressure builds up and heat dissipation inefficiency, high temperature may occur in the battery. With the battery system that experiencing an exothermic reaction, pressure fluctuations will accelerate the reaction rate, and further intensify the heat production. Thus, it is crucial to monitor the pressure within the battery as a means of preventing rapid temperature escalation that could trigger a thermal runaway event. Cai T. *et al.*, [3] in their work have suggested to place the pressure sensor inside the vent channel found in battery packs. as shown in Figure 1. This study will present the design and analysis of appropriate MEMS capacitive pressure sensor to be utilized for monitoring the internal pressure of the battery.

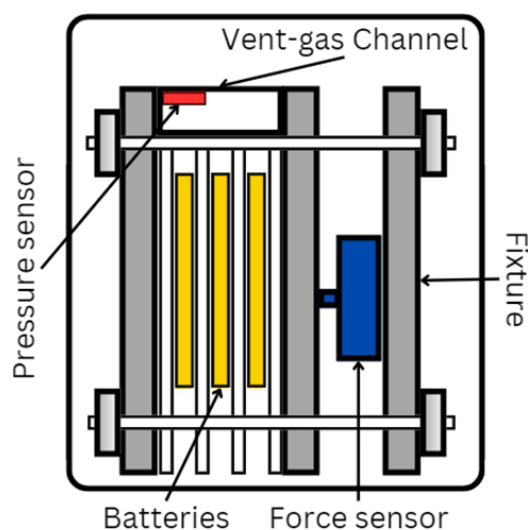


Figure 1. Suggestion of pressure sensor location [3].

1.1 Theoretical of MEMS Capacitive Pressure Sensor Design

Capacitive pressure sensors detect atmospheric pressure by measuring the change in capacitance caused by the deformation of a diaphragm due to applied pressure. The diaphragm of the sensor is required to be exposed to the ambient air, to allow it to be directly influenced by the atmospheric pressure.

As the atmospheric pressure changes, the diaphragm of the sensor undergoes slight deflection, causing a modification of the distance between the diaphragm and a stationary plate or electrode. This change in distance leads to a variation in the capacitance of the sensor as defined by the common capacitance equation as in Eq. 1. where C is the capacitance in Farad, ϵ is the permittivity of the dielectric, A is the area of overlapped electrode and d is the distance between the diaphragm and the stationary plate or electrode. The electrical signal generated by the sensor is subsequently processed and calibrated to provide an accurate measurement of atmospheric pressure.

$$C = \frac{\epsilon A}{d} \quad (1)$$

Figure 2 shows the working principle of a common MEMS capacitive pressure sensor. When electrostatic force is applied to the diaphragm, the distance between the diaphragm and a stationary plate or electrode will be reduced and this is translated to the changes in the capacitance value.

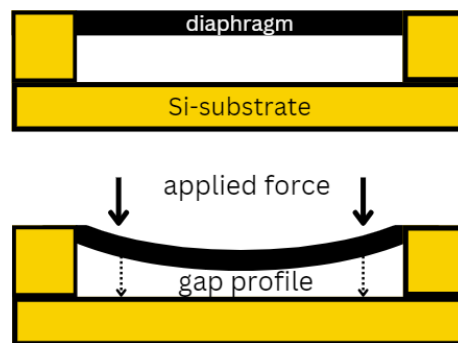


Figure 2. Working principle of common MEMS capacitive pressure sensor [4].

Since previous researchers had proven that the device sensitivity of the pressure sensor can be enhanced through a slotted-square design [5], this work will be focusing in investigating the sensitivity of three different square slotted diaphragms design namely clamped-square, four-slotted-square and eight-slotted-square designs of MEMS capacitive pressure sensor.

At rest position, the capacitance value of the MEMS capacitive pressure sensor is given by Eq. 1 where C_t is the total capacitance and x is the displacement of the diaphragm from its initial position. When voltage is applied between the two plates, the capacitance value will be determined by using Eq. 2.

$$C = \frac{\epsilon A}{d-x} \quad (2)$$

The sensor's ability to detect displacement, denoted as S_z , is derivable from the change in C_t with respect to the displacement direction, z . Equation 3 outlines how the displacement sensitivity of the engineered sensor is defined.

$$S_z = \frac{\partial C_t}{\partial z} \quad (3)$$

2. MASK DESIGNS AND METHODS

A clamped-square, four-slotted-square and eight-slotted-square pressure sensors layouts were designed using Intellisuite's Blueprint module. Figure 3 shows the mask of all three designs and their parameters. The slotted type designs were adapted based on research work reported by Nallathambi *et al.* [5]. They have reported that the slotted-type diaphragm that they designed has better sensitivity as compare to the square type diaphragm.

Microfabrication process steps of the MEMS capacitive pressure sensor were defined in the Intellisuite's FabSim module. Table 1 shows the details of the processes that inclusive of the total of 14 steps. Type of processes, materials used, and material thicknesses are among the details that can be extracted from Table 1.

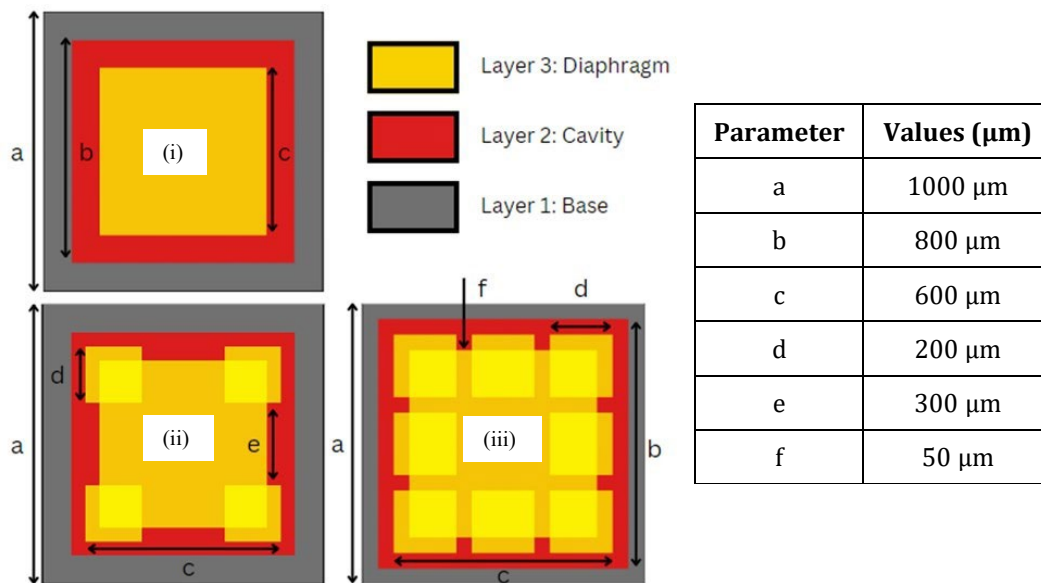


Figure 3. Mask layout design for (i) clamped-square, (ii) four-slotted-square and (iii) eight-slotted-square pressure sensors.

Table 1 The Details of the Microfabrication Processes

Step	Type	Material	Process	Pro. ID	Pro. Option	Thickness μm
1	Definition	Si	Czochralski	Generic		10000
2	Deposition	Si	PECVD	Generic	Conformal Deposition	100
3	Deposition	PSG	Generic	Generic	Conformal Deposition	10000
4	Deposition	PR-AZ5214	Spin	001	Conformal Deposition	300
5	Exposure	UV	Contact	Suss		
6	Etch	PSG	Wet	Generic	Partial Etching	10000
7	Etch	PR-AZ521	Wet	1112A	Partial Etching	300
8	Deposition	PSG	Generic	Generic	Conformal Deposition	10000
9	Deposition	PR-AZ5214	Spin	001	Conformal Deposition	300
10	Exposure	UV	Contact	Suss		
11	Etch	PSG	Wet	Generic	Partial Etching	10000
12	Etch	PR-AZ5214	Wet	112A	Partial Etching	300
13	Deposition	PolySi	LPCVD	SiH ₄	Conformal Deposition	10000
14	Etch	PSG	Wet	Generic	Sacrifice	

Fabrication process steps of the MEMS capacitive pressure sensor were defined in the Intellisuite's FabSim module. Design process started with layout drawing and following by the definition of microfabrication process in order to generate the 3-D model of the MEMS capacitive pressure sensor. The top-view and cross-section of the 3D model of the designed clamped-square, four-slotted-square and eight-slotted-square pressure sensors are shown in Figure 4 (a), (b) and (c) respectively.

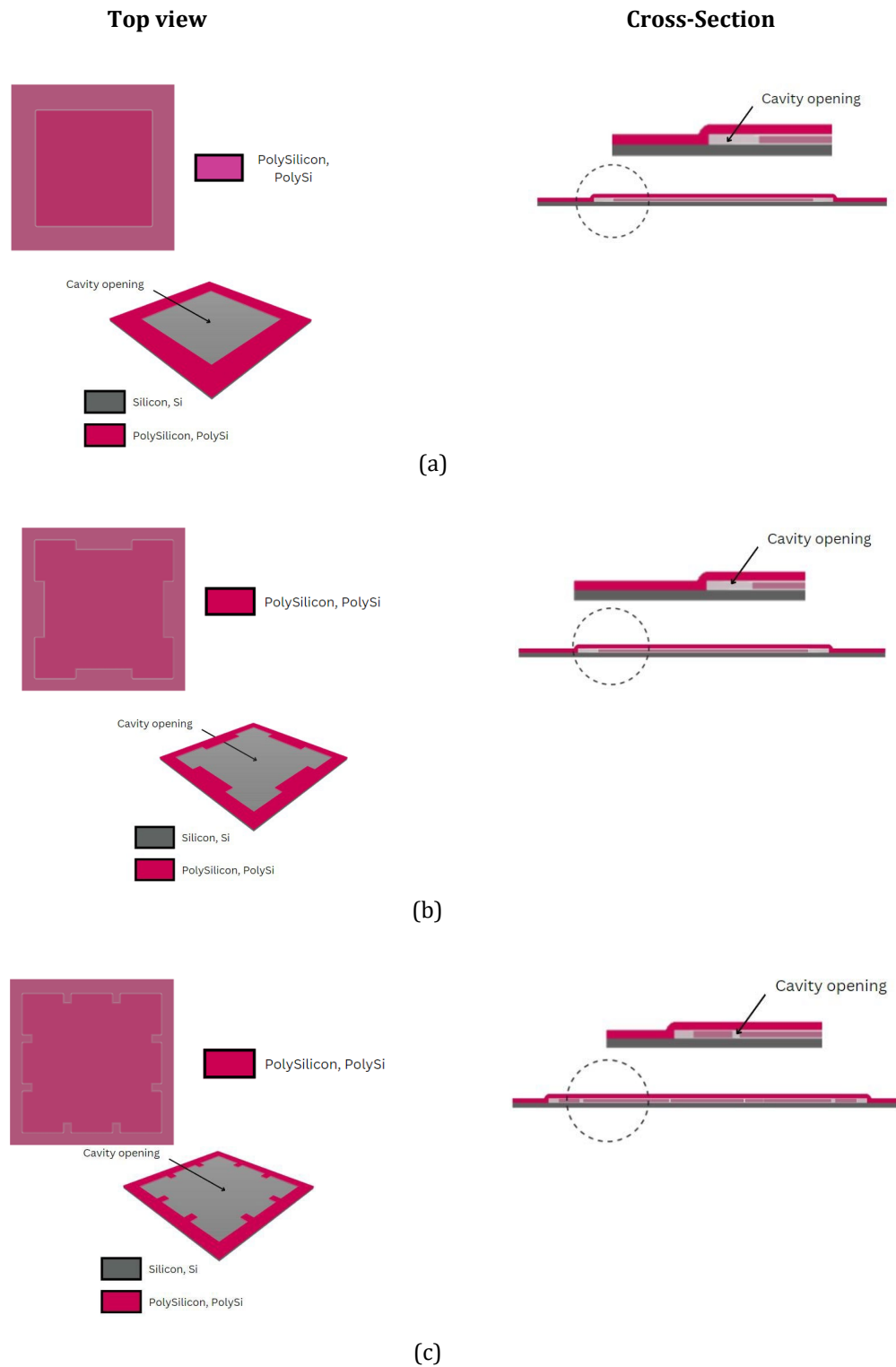


Figure 4. Top view and cross-sections of (a) Clamped-square MEMS capacitive pressure sensor (b) Four-slotted-square MEMS capacitive pressure sensor, and (c) Eight-slotted-square MEMS capacitive pressure sensor.

Upon generating the 3D model, the next step involves meshing and then exporting the model to the TEMAnalysis module for the purpose of conducting simulation and subsequent analysis. The simulation will be involving diaphragm simulation, and the overall MEMS capacitive pressure sensor.

2.1 Diaphragm Simulation Setting


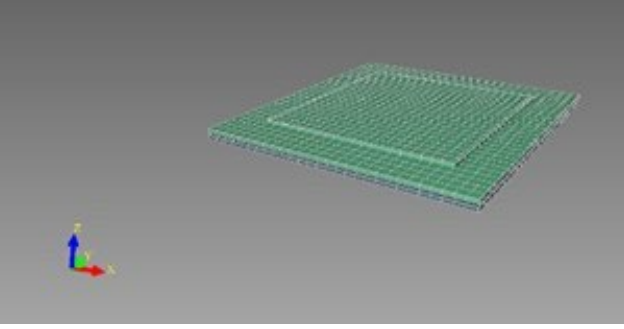

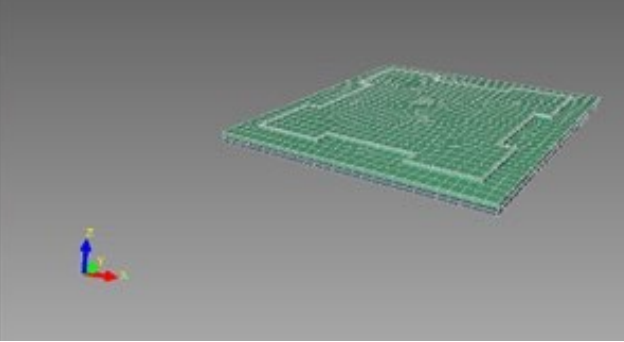
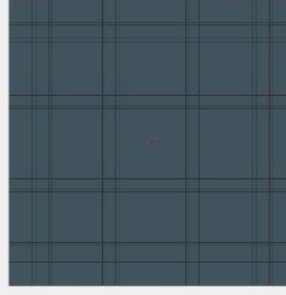
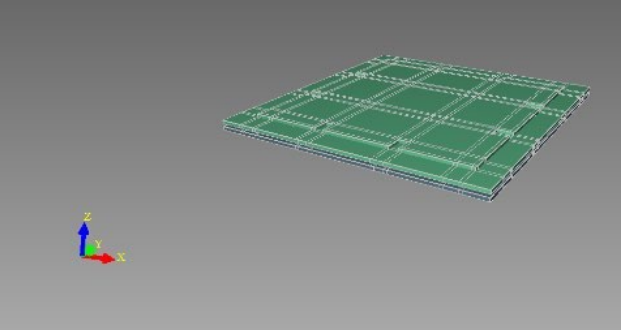
This simulation explores the idea of enhancing sensitivity by introducing slots into the diaphragm layout. Specifically, the focus of this simulation is solely on the diaphragms themselves, and this sub-topic describes the simulation setting for the diaphragm. Table 2 shows the simulation settings and parameters that applied identically to all three designs i.e. clamped-square, four-slotted-square and eight-slotted-square. Based on findings presented in the research conducted by C. Fang *et al.* [6], which highlight the optimal pressure parameter as 0.35 MPa in the lithium metal batteries, this study employed a peak pressure of 0.35 MPa on both the diaphragm and the MEMS capacitive pressure sensor.

Table 2 Diaphragm simulation setting and parameters for all three designs

Module	Parameter	Values
3D Builder	Layer height	Layer 0 = 10 μm Layer 1 = 10 μm
	Mesh engine	Manhattan
	Mesh size	30 μm
TEMAalysis	Simulation setting	Static: Stress/Displacement
	Material:	Polysilicon, PolySi
		0.10
		0.15
	Load: Pressure (MPa)	0.20
		0.25
	0.30	
		0.35

Table 3 illustrates the utilization of 3D Builder to designate specific layers as entities, with the layer height modified to 10 μm . Furthermore, extra empty space was introduced at Level 2 to facilitate the observation of diaphragm deformation during the simulation process. Meshing was performed with a minimum spacing of 30 μm .

Table 3 Model modification using 3D builder

Design Type	Final Output	
Clamped-square		
Four- slotted squareshape		
Eight- slotted square shape		

2.2 MEMS Capacitive Pressure Sensor Simulation Setting

Following the simulation of the diaphragm in sub-section 2.1, the complete MEMS capacitive pressure sensor is subsequently simulated using the parameters outlined in Table 4.

Table 4 MEMS Capacitive pressure sensor simulation setting and parameters

Module	Parameter	Values	
3D Builder	Layer height	Layer 0 = 10 μm	
		Layer 1 = 10 μm	
		Layer 2 = 10 μm	
		Layer 3 = 10 μm	
	Mesh engine	Manhattan	
	Mesh size	30 μm	
Static: Thermoelctromechanical Relaxation.			
	Simulation setting	Contact Analysis	
	Material:	Entity 1: POLYSILICON, POLYSI	Entity 2: Silicon, Si
<u>TEMAnalysis</u>	Load: Voltage	Entity 1: 0V	Entity 2: 1 to 5 V
		0.00 - 0.10	
	0.10 - 0.15		
	0.15 - 0.20		
	Load: Face No. 22 Pressure (MPa)	0.20 - 0.25	
		0.25 - 0.30	
0.30 - 0.35			

Before applying voltage and pressure loads to the structure, it is necessary to establish the boundary conditions, which involve configuring fixed faces and defining contact pairs.

3. RESULTS AND DISCUSSION

3.1 Diaphragm Simulation Results

The first set of results to be discussed in this section are the displacement of the diaphragm under different loading conditions. The applied load encompassed pressures spanning 0.1, 0.15, 0.2, 0.25, 0.3, and 0.35 MPa. The geometry underwent deformation, leading to displacements from the original position, as shown in Table 5, 6 and 7 for clamped-square, four-slotted-square and eight-slotted-square designs respectively. Notably, the most substantial displacements are highlighted in a red hue. The 3D visual representations remain consistent across each pressure level.

Table 5 3D visualization of displacement result for clamped-square design

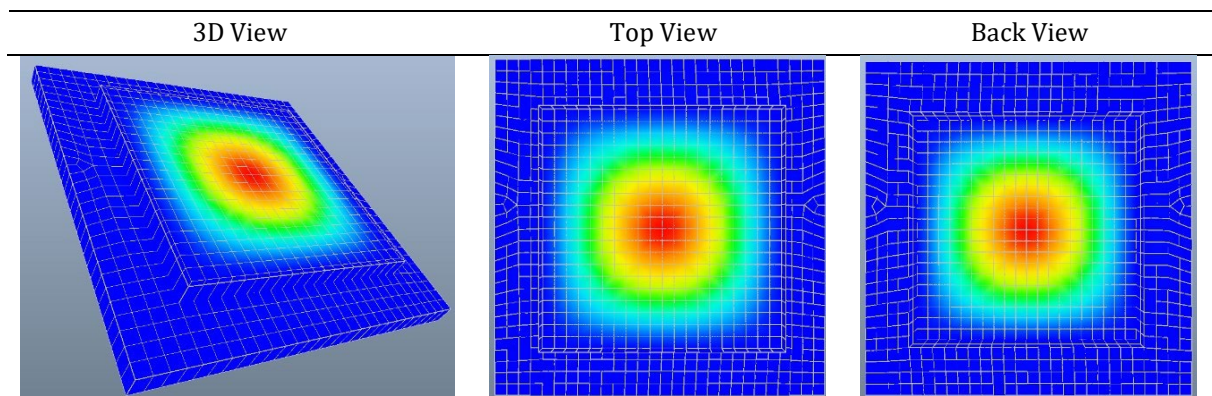


Table 6 3D visualization of displacement result for four-slotted-square design

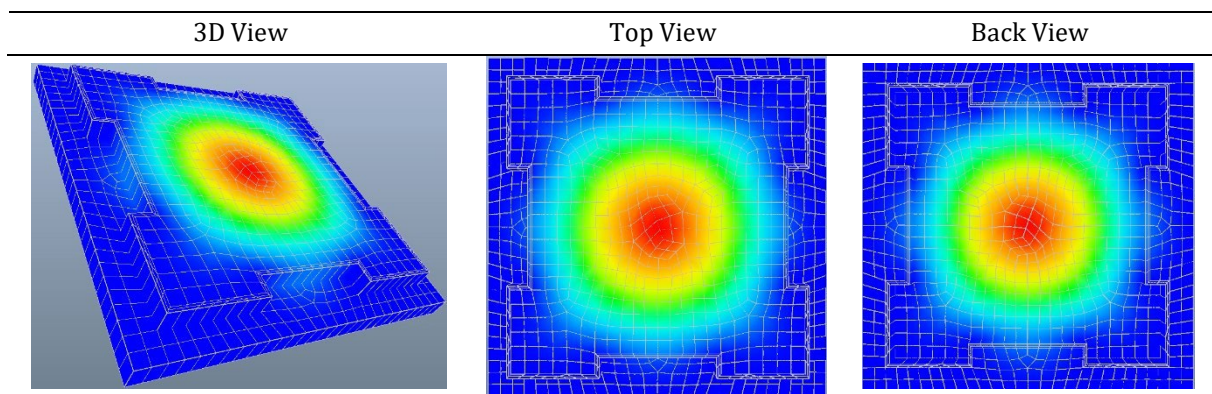
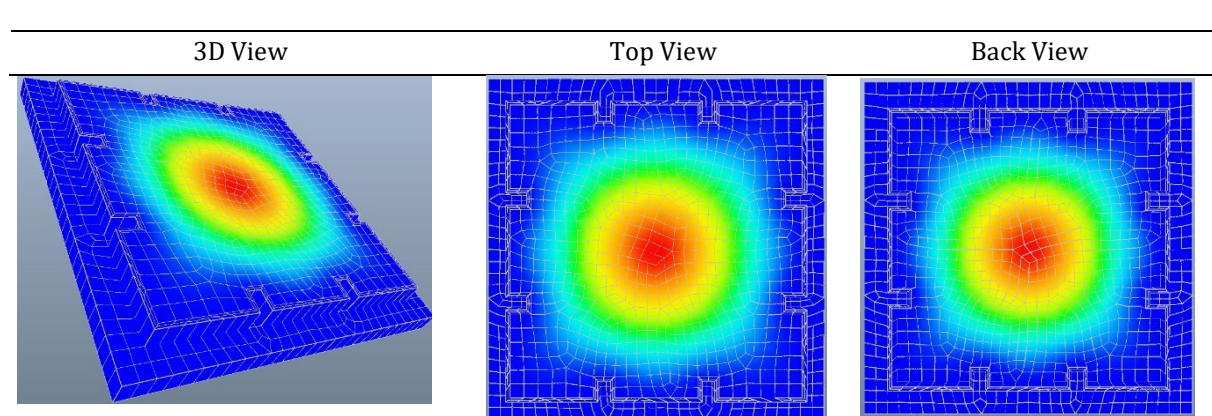


Table 7 3D visualization of displacement result for eight-slotted-square design



To facilitate an understanding of the displacement range, measurements are presented in graph form, as shown in Figure 5, 6 and 7 for clamped-square, four-slotted-square and eight-slotted-square designs respectively.

As can be seen from Figure 5, the displacement of the diaphragm is directly proportional with pressure that applied to the structure. When subjecting the clamped-square diaphragm to a peak pressure of 0.35 MPa, it leads to a maximum diaphragm displacement of 4.386 μm .

The four-slotted square design displacement has also direct correlation to the applied pressure. When subjected to the identical peak pressure of 0.35 MPa, the diaphragm underwent its highest displacement of 5.395 μm .

As predicted earlier, when subjected to a peak pressure of 0.35 MPa, the eight-slotted square design exhibited the greatest diaphragm displacement, measuring 5.507 μm .

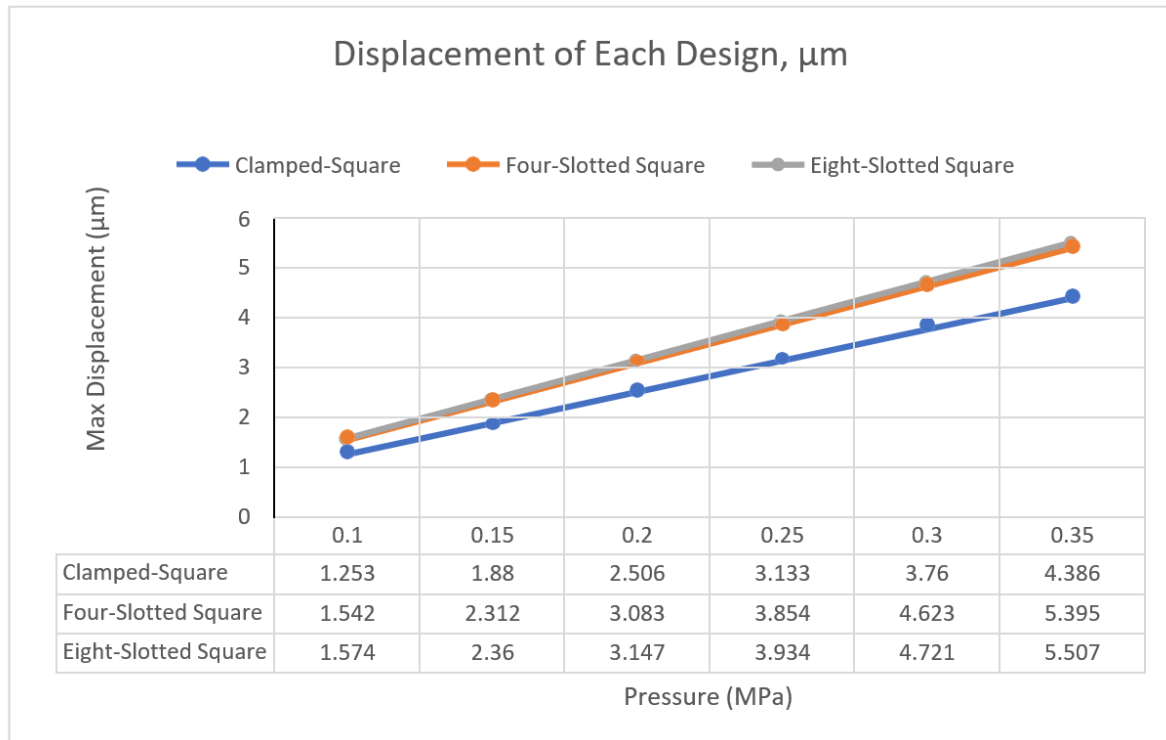
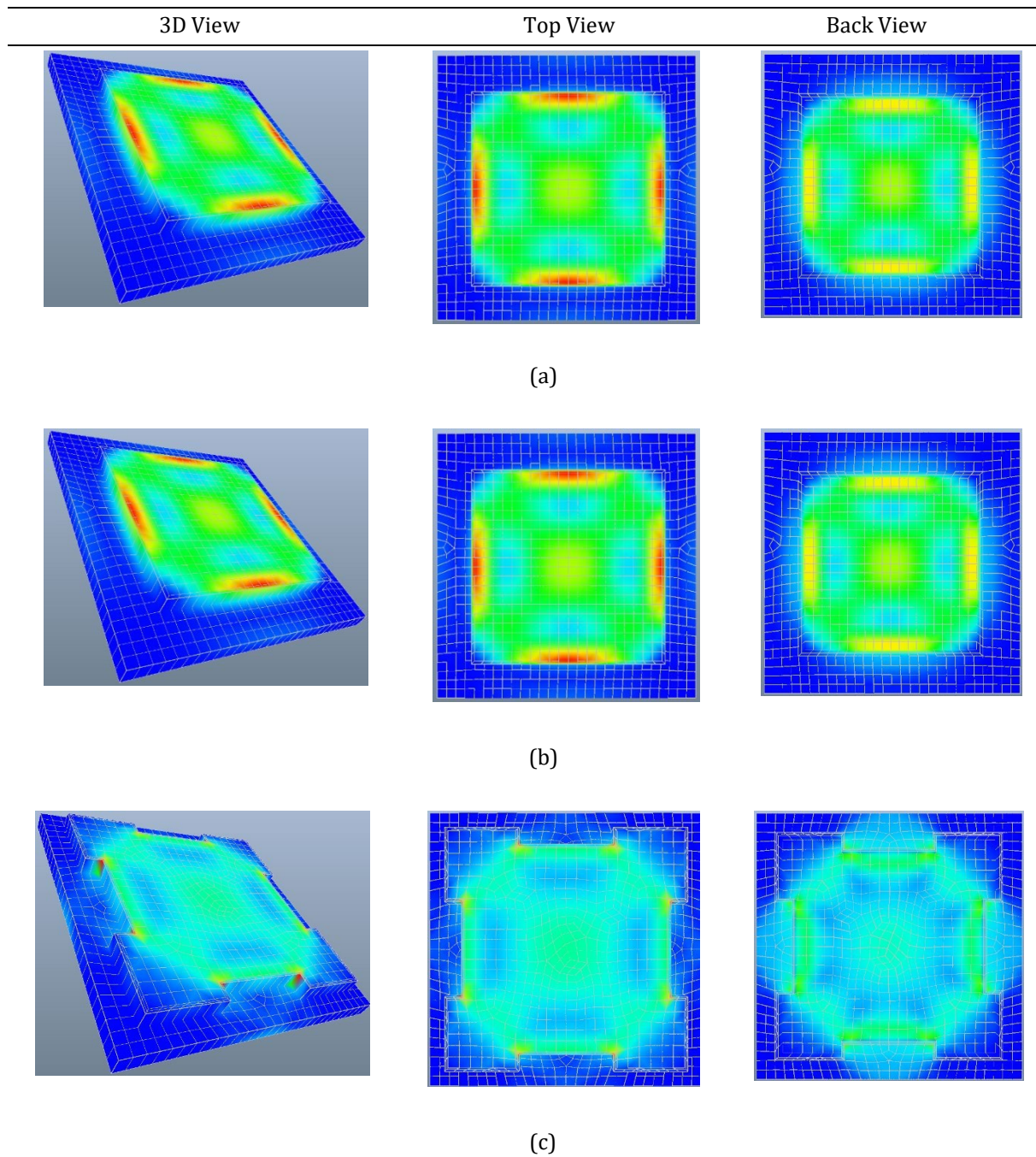


Figure 5. Displacement for clamped-square, four-slotted-square and eight-slotted square diaphragm design under various load.

Subsequently, we will analyse the distribution of Mises stress on the diaphragms resulting from the application of various pressures across all three design configurations. The stress distribution will be depicted through both 3D visualization and graphical representation.

Table 8 presents the 3D visual representations of Mises stress distribution on the diaphragms across three design configurations: (a) clamped-square, (b) four-slotted-square, and (c) eight-slotted-square. These visualizations correspond to different applied pressure levels: 0.1, 0.15, 0.2, 0.25, 0.3, and 0.35 MPa. Red hue indicates the area with the highest stress experienced by the geometry when load is applied.

Table 8 3D visualization of Mises stress distribution for (a) clamped-square, (b) four-slotted-square and (c) eight-slotted-square designs



As shown in Figure 6, the highest value of Mises stress was also observed when the maximum peak pressure of 0.35 MPa was applied to all three design configurations: clamped-square, four-slotted-square, and eight-slotted-square. For the clamped-square, the maximum Mises stress obtained when 0.35 MPa applied is 294.39 MPa, while for the four-slotted-square, and eight-slotted-square diaphragms, the maximum Mises stress obtained are 543.69 MPa and 644.67 MPa respectively.

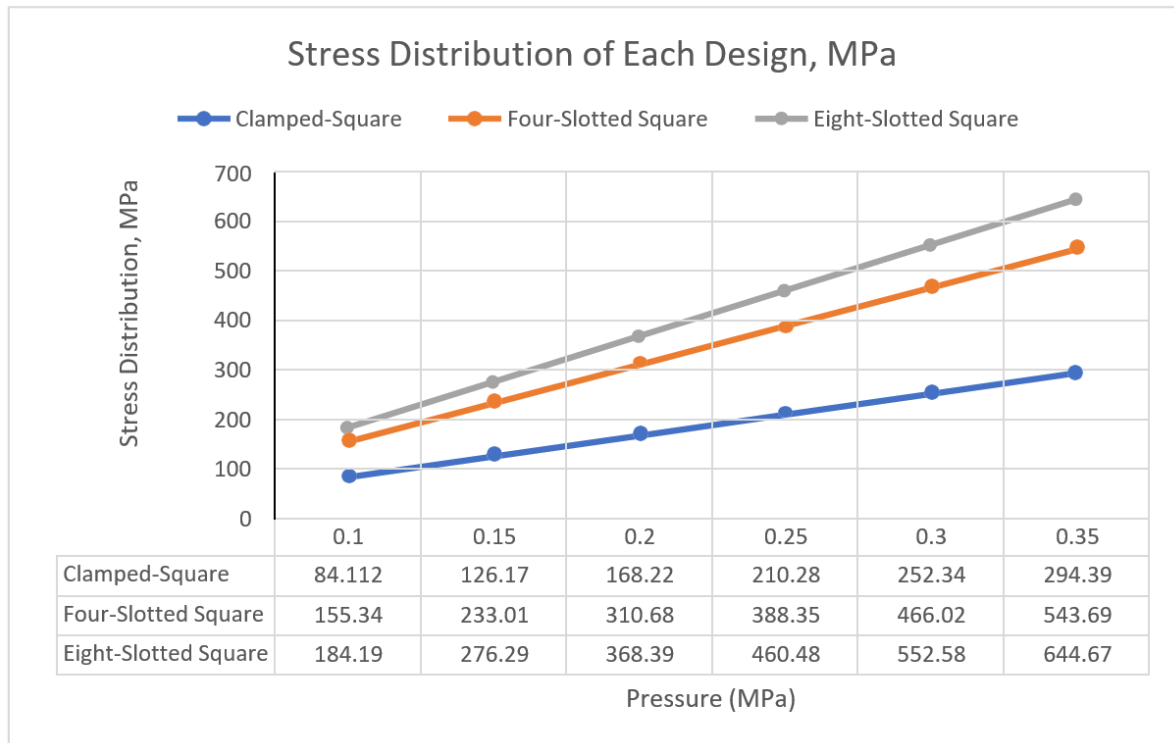
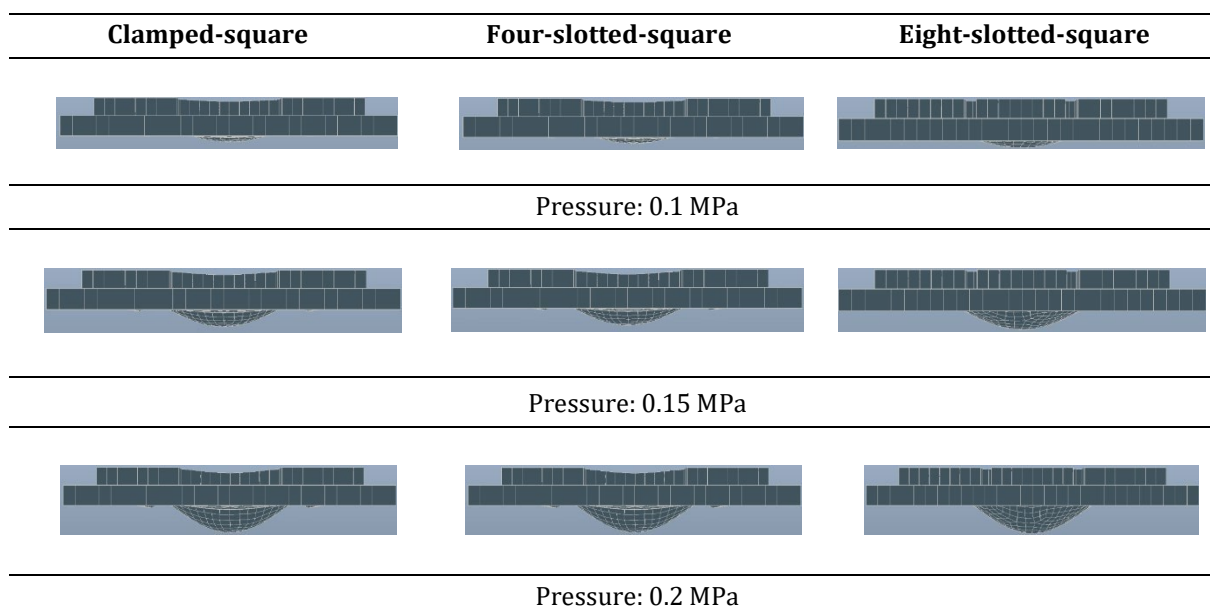


Figure 6. Mises stress distribution for clamped-square diaphragm.

The influence of applying different pressures to the diaphragm's shape deformation can also be observed using the simulation tool. Figure 7 shows the deformed shape of all three designs, when the pressure is applied within 0.1 until 0.35 MPa. In order to enhance the visibility of the deformed shape, the scale factor was set to 10 for every load parameter.

The variation in the deformed shape between the square shape that is clamped and the square shape with four slots demonstrates nearly identical results. However, the distorted configuration achieved through the square shape with eight slots appears noticeably higher when compared to the other two designs.



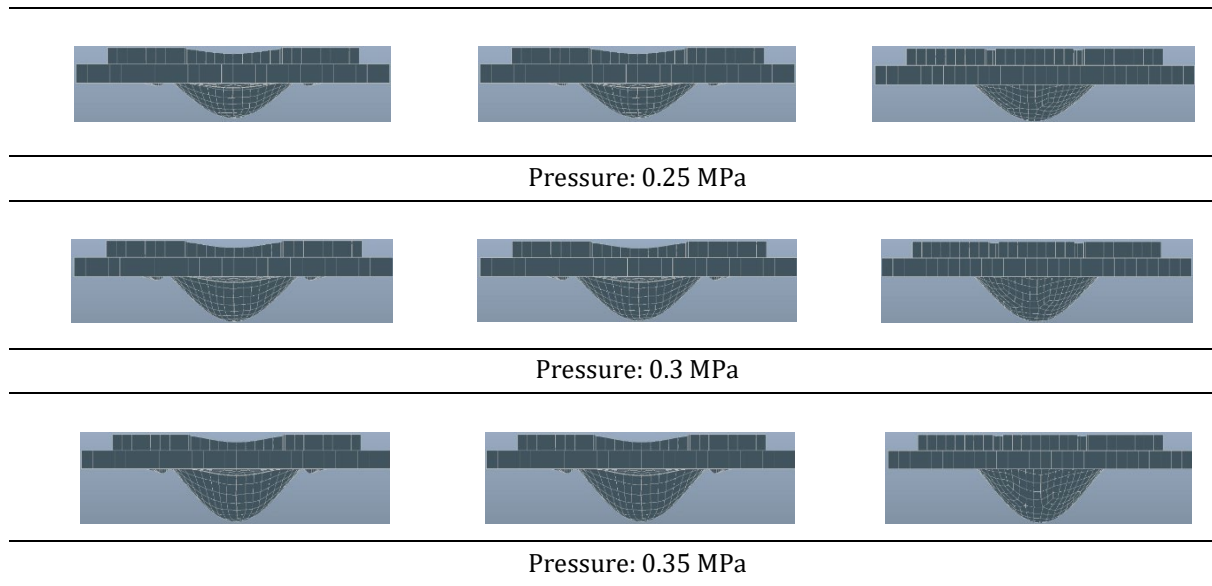


Figure 7. The deformed shape of all three diaphragm designs, i.e. clamped-square, four-slotted- square, and eight-slotted-square when pressure applied from 0.1 until 0.35 MPa.

3.1 MEMS Capacitive Pressure Sensor Simulation Results

Utilizing the simulation configurations outlined in section 2.2, various outcomes including capacitance, and sensitivity of the MEMS capacitive pressure sensor will be obtained through TEMAnalysis. The simulation of the maximum displacement and the Mises stress distribution in the upper movable electrode will not be re-executed, as these values are expected to correspond with the results obtained from the diaphragm simulation.

The mechanical sensitivity of the MEMS capacitive pressure sensor was determined in this study using Equ. 4 which is adapted from [7].

$$\frac{\text{Displacement } (\mu\text{m})}{\text{Pressure (MPa)}} = \text{Sensitivity } (10^{-12}/\text{Pa}) \quad (4)$$

From the data depicted in Figure 8, the pressure sensor featuring an eight-slotted square diaphragm achieved the greatest mechanical sensitivity when compared to those with clamped-square and four-slotted-square diaphragms. However, the pressure sensor employing the four-slotted square diaphragm exhibited a nearly equivalent mechanical sensitivity, with a marginal variance of approximately 1.87% at the optimized pressure peak of 0.35 MPa.

The results are in accordance with the predictions, as depicted in Figure 5, where the pressure sensor with eight slots exhibited a greater displacement compared to the other two designs during simulation.

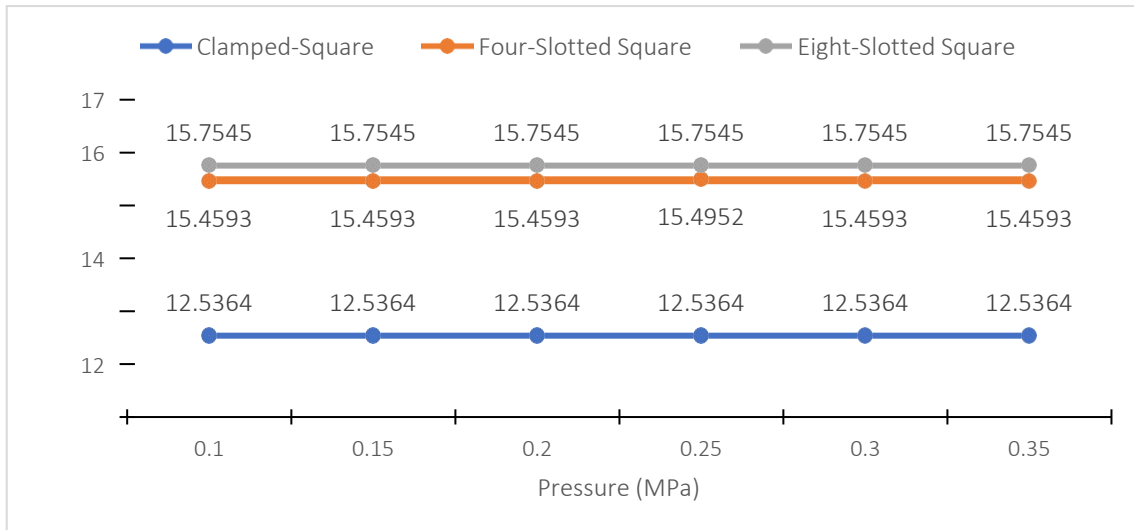


Figure 8. Mechanical sensitivity of the MEMS capacitive pressure sensor.

Moreover, the capacitance as one of the essential values for the MEMS capacitive pressure sensor is further investigated in this section. Table 9 presents the maximum achievable capacitance values under various applied pressures to the sensor. In theoretical terms, as the movable electrode draws closer to the fixed electrode, the gap between them narrows, leading to an increase in capacitance. However, this scenario does not happen in the current context, as the modification of the overlapped area between the upper and lower electrodes is reduced by the slotted square plate. We can see from Table 9 that the capacitance between all three designs is close to each other but sensor with clamped-square diaphragm obtained the highest if compared to the sensor with four-slotted-square and eight-slotted-square diaphragms. When the optimized peak pressure of 0.35 MPa is applied to all the design, clamped-square sensor yielded 0.5410 μF , four-slotted square with 0.5192 μF and eight-slotted square obtained 0.5008 μF .

Table 9 MEMS capacitive pressure sensor simulation setting and parameters

Load pressure (MPa)	Max Capacitance (μF)		
	Clamped-Square	Four-Slotted Square	Eight-Slotted Square
0.00 to 0.1	0.5316	0.5043	0.4868
0.1 to 0.15	0.5334	0.5071	0.4892
0.15 to 0.2	0.5352	0.5099	0.4919
0.2 to 0.25	0.5370	0.5128	0.4946
0.25 to 0.3	0.5390	0.5160	0.4976
0.3 to 0.35	0.5410	0.5192	0.5008

4. CONCLUSION

Based on simulations results obtained from this work, it can be concluded that the MEMS capacitive pressure with eight-slotted square displayed remarkable performance in terms of displacement, Mises stress, and mechanical sensitivity when compared to clamped-square and four-slotted square designs. By subjecting all three designs with optimized peak pressure of 0.35

MPa, the eight-slotted design exhibits a displacement of 5.507 μm , the highest Mises stress of 644.67 MPa, and as well as the highest mechanical sensitivity at 15.7545 (10-12/Pa). However, it's important to note that the introduction of slots had a negative impact on the capacitance value. It was found that the eight-slotted yielded only 0.5008 μF , as compared to the clamped-square sensor that yielded 0.5410 μF , and four-slotted square with 0.5192 μF . Incorporating an eight-slotted diaphragm into the pressure sensor design proves beneficial for enhancing displacement and consequently sensitivity. Nonetheless, a disadvantage arises with the eight-slotted design in the form of a diminished capacitance value caused by the decrease in the overlapped area, which directly influences the capacitance measurement.

ACKNOWLEDGEMENTS

Thank you to the Faculty of Electronic Engineering & Technology, UniMAP for providing simulation facilities used in this work.

REFERENCES

- [1] Electric Car Sales and Statistics for 2022, Tridenstechnology.com, Dec. 08, 2022. <https://tridenstechnology.com/electric-car-sales-statistics/> (accessed Dec. 29, 2023).
- [2] P. Sun, R. Bisschop, H. Niu, & X. Huang, 2020, *Fire Technol*, 1–50.
- [3] Ting Cai, Peyman Mohtat, Anna G. Stefanopoulou, Jason B. Siegel, 2020, *IFAC-PapersOnLine*, **53**, Issue 2, 12491-12496.
- [4] A. Sharma & J. Singh, 2013, Design and analysis of high performance MEMS capacitive pressure sensor for TPMS, in 2013 International Conference on Control, Automation, Robotics and Embedded Systems (CARE), Jabalpur, India, pp. 1-5.
- [5] N. Arjunan & T. Shanmuganatham, 2015, *ICTACT Journal on Microelectronics*, 01 (Jul.), 62–67.
- [6] C. Fang *et al.*, 2021, *Nat Energy*, vol. **6**, no. 10, 987–994.
- [7] B. A. Ganji & M. Shams Nateri, 2013, *IJE Transactions B: Applications*, Vol. **26**, No. 11, 1331-1336.